IEEE Access
Multidisciplinary | Rapid Review | Open Access Journal

Received 12 January 2024, accepted 29 January 2024, date of publication 13 February 2024, date of current version 20 February 2024.

Digital Object Identifier 10.1109/ACCESS.2024.3365502

RESEARCH ARTICLE

Non-Cascaded Sensorless Control of SPMSM Based on Cascaded Extended State Observer

LIJUN CHEN[1], (Student Member, IEEE), DONGLIANG LIU[1,2], MINCHEN ZHU[1], LILI CUI[1], LIMIN SUN[1], CHENGGEN ZHAN[1], AND HENG SHI[1]

[1]Zhejiang IoT Perception and Information Fusion Technology Key Laboratory, Hangzhou Dianzi University, Hangzhou 310000, China
[2]Wolong Electric Group Company Ltd., Shaoxing, Shangyu 312300, China

Corresponding author: Dongliang Liu (liudl@hdu.edu.cn)

This work was supported in part by the National Natural Science Foundation of China under Grant 51877059.

ABSTRACT Attaining precise and dynamic speed control is pivotal for the efficient sensorless operation of permanent magnet synchronous motors. Addressing the challenge of parameter mismatch within the cascaded control structure of these motors, which results in diminished dynamic performance and increased static deviation, this paper introduces a speed-current single-loop control method for permanent magnet synchronous motors based on non-singular terminal sliding mode control. To begin, a second-order mathematical model of the motor under parameter disturbances is analyzed and derived. To suppress system disturbances arising from parameter mismatches, a cascaded extended state observer is established. A ultra-local model of the motor is then derived based on the mathematical model, and an adaptive non-singular fast terminal sliding mode controller is designed. The proposed method aims to optimize dynamic performance, steady-state accuracy, and system robustness. Finally, a rigorous stability analysis has been conducted for the proposed composite strategy. The feasibility and effectiveness of this approach are verified through comparative experiments with PID and sliding mode control (SMC).

INDEX TERMS Speed-current single-loop control, adaptive non-singular fast terminal sliding mode controller, permanent magnet synchronous motor, cascade extended state observer.

I. INTRODUCTION

Permanent magnet synchronous motor (PMSM) are widely used in aerospace, defense, and electric vehicles due to their high power density, torque output, and broad speed range [1], [2], [3]. The integration of sensorless control in PMSM drives has garnered significant attention as it eliminates the need for position sensors, leading to cost reduction, improved reliability, and enhanced robustness. Consequently, sensorless control techniques have become a prominent research focus in electric propulsion systems [4].

Sensorless control of permanent magnet synchronous motor (PMSM) employs different methods to acquire rotor position information based on the operating speed. At low speeds, the convex polarity of the rotor enables high-frequency injection for position estimation [5], [6]. At high speeds, mathematical models and observers such as sliding mode observer, model-referenced adaptive observer, and flux observer are utilized for rotor position estimation [7], [8], [9]. Traditional sensorless control approaches often rely on PID control in the speed and current loops. However, due to the nonlinearity, strong coupling, and time-varying parameters of PMSM drive systems, PID control may not guarantee satisfactory dynamic performance [10]. On the other hand, model predictive control (MPC) offers simplified modeling and robustness but requires significant computational resources [11]. In recent years, higher-order non-singular terminal sliding mode control has gained attention for its desirable features, including fast convergence even when the system state is far from the origin, global convergence, and insensitivity to parameter variations and disturbances [12].

In recent years, there has been a growing interest in non-cascaded control strategies for permanent magnet synchronous motor drive systems, aiming to reduce the control cycle difference between the speed and current loops

The associate editor coordinating the review of this manuscript and approving it for publication was Ton Duc Do.

and eliminate the cascade structure. These non-cascaded approaches offer advantages such as simplified control structure and direct speed control.

Several studies have explored non-cascade control methods for PMSM systems. For example, in [13], a non-cascaded model-free predictive speed control method is proposed using composite variables to build a ultra-local model. The Lyapunov function ensures global convergence. Similarly, in [14], a finite control set strategy is introduced for a dual permanent magnet motor system using a non-cascaded structure to predict the reference voltage vector based on current and speed information. In [15], a fuzzy non-cascaded speed control scheme based on a virtual reference is proposed. The scheme uses a fuzzy disturbance observer to estimate the mismatched load torque and a novel virtual reference planner for feedback compensation to ensure conservative closed-loop stability. Furthermore, in [16], a control law is developed from a sliding modal surface under a non-cascaded structure, which establishes a ultra-local model and enhances the system robustness. In [17], a speed-current single-loop controller was designed for a PMSM drive system using a nonlinear disturbance observer to estimate the disturbances. Although the non-cascade control shows good promise for PMSM systems, further improvements are needed to improve the speed dynamic response and immunity to perturbations.

Anti-interference performance is a critical concern in non-cascaded control structures for permanent magnet synchronous motor systems. PMSM drive systems face challenges such as unmodeled dynamics, time-varying parameters, and torque variations, which hinder the establishment of accurate mathematical models [18], [19]. To address these challenges, various methods have been proposed for disturbance observation, including the sliding mode observer, disturbance observer, luenberger observer, and extended state observer. However, each method has its limitations. The sliding mode observer requires highly accurate model parameters and is suitable for handling specific types of disturbances [20]. The disturbance observer's performance relies heavily on the spectral characteristics of the disturbance signal, making it less effective for complex or uncertain disturbance signals [21]. The luenberger observer imposes strict requirements on the system's dynamic characteristics, which may limit its performance in the presence of uncertain or highly variable motor dynamics [22]. In contrast, the extended state observer offers several advantages, including reduced model dependence, faster response times, and improved estimation accuracy. By incorporating information about system dynamics and disturbances, the extended state observer provides a more adaptable and robust approach for handling disturbances in PMSM systems. In summary, the extended state observer shows promise in enhancing the anti-interference performance of non-cascaded control structures in PMSM systems. Its ability to handle unmodeled dynamics and disturbances more effectively contributes to improved system performance and stability.

Speed dynamic response is a key aspect of non-cascade control in permanent magnet synchronous motor (PMSM) systems. In [23], a single-loop speed-current control strategy is presented, employing continuous integral terminal sliding mode control and a perturbation observer. This approach adopts a non-cascaded structure and develops a nonlinear motor model that considers superimposed perturbations. By introducing a virtual control component, a continuous integral sliding mode controller is designed to achieve global asymptotic stability based on the Lyapunov criterion. In [24], a backstepping non-vectorized terminal sliding mode control technique with a finite-time disturbance observer is utilized. Furthermore, in [25], a new non-vector fast terminal sliding mode control algorithm called NFTSM is proposed. NFTSM demonstrates faster response, no overshoot, improved interference immunity, and reduced jitter.

This paper presents a novel approach for the control of surface-mounted permanent magnet synchronous motor (SPMSM) drives, with a particular focus on achieving high-speed dynamic performance and robustness. The main innovative contributions of this research are as follows:

1) Based on the premise of a ultra-local model, a novel adaptive high-order non-singular terminal sliding mode controller is designed. Operating within a non-cascade control structure, this controller can effectively regulate both speed and current. It significantly reduces speed errors and enhances the response speed and robustness of the SPMSM drive system, even in the presence of uncertainties and variations.

2) Introduced is a cascaded extended state observer for real-time disturbance handling. This observer accurately observes and compensates for disturbances, effectively suppressing harmonics and further enhancing the system's performance and stability.

3) Experimental Validation: Extensive experimental tests have been conducted to validate the effectiveness of the proposed method. The experimental results demonstrate significant improvements in speed dynamic performance and robustness, highlighting the practical applicability of the approach.

In summary, this research offers a novel non-cascade control method for SPMSM drives, incorporating an adaptive non-singular terminal sliding mode controller and a cascaded expansion state observer. The experimental validation confirms the effectiveness of the proposed approach in achieving superior speed dynamic performance and robustness.

II. PRINCIPLE ANALYSIS OF PERMANENT MAGNET SYNCHRONOUS MOTORS

A. SPEED ESTIMATION SCHEME BASED ON QPLL

The expression of the flux of the permanent magnet in the stationary coordinate system is:

$$\begin{cases} \eta(\hat{x}_1) = \psi_f cos\theta_e \\ \eta(\hat{x}_2) = \psi_f sin\theta_e \end{cases} \tag{1}$$

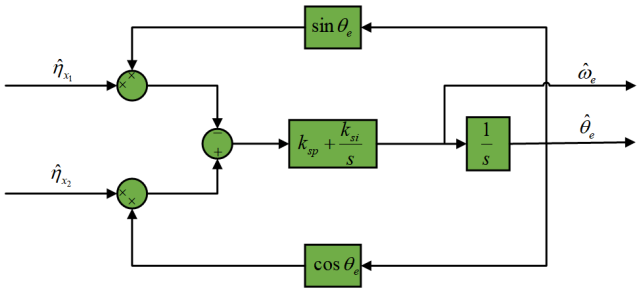

FIGURE 1. Basic principle diagram of QPLL.

where $\hat{\eta}_1$, $\hat{\eta}_2$ are the flux under the α and β axes, and θ_e is the electrical angle of the motor, respectively.

Let's take a closer look at the fundamental principle of the Q-PLL. Using the flux observer as an illustration, the QPLL is designed to extract the positional information encoded within the phase of the rotor flux. The angular error is computed using the formula:

$$\begin{aligned}\Delta\theta_e &= \eta(\hat{x}_2)cos\hat{\theta}_e - \eta(\hat{x}_1)sin\hat{\theta}_e \\ &= \psi_f sin\theta_e cos\hat{\theta}_e - \psi_f sin\hat{\theta}_e cos\theta_e \\ &= \psi_f sin(\theta_e - \hat{\theta}_e) \\ &\approx \theta_e - \hat{\theta}_e \end{aligned} \tag{2}$$

The angular error is processed through the PI loop to calculate the angular velocity, represented as ω_e. The expression is given by the equation:

$$\omega_e = k_{sp} \cdot \Delta\theta_e + \int k_{si} \cdot \Delta\theta_e \tag{3}$$

The basic schematic of the QPLL is shown in figure 1. The scheme takes the estimated rotor flux as input. In the figure 1, k_{sp}, k_{si} are the proportional gain, the integral gain, and finally the error of the electrical angle obtained from the QPLL can be made to converge to 0.

B. MATHEMATICAL MODELLING OF PERMANENT MAGNET SYNCHRONOUS MOTORS

Mechanical equations of motion for permanent magnet synchronous motors:

$$\begin{cases} J\dfrac{d\omega_e}{dt} = T_e - T_L - B\omega_e \\ T_e = \dfrac{3n_p\psi_f}{2} i_q \end{cases} \tag{4}$$

where, ω_e is the speed of the motor; ψ_f is the flux of the motor; T_e is the electromagnetic torque; T_L is the load torque; B is the viscous coefficient; J is the rotational inertia; n_p is the pole pair number; and i_q is the q-axis current.

In the dq coordinate system with synchronous speed rotation, the dynamic equation of the PMSM drive system current is:

$$\begin{cases} \dfrac{di_d}{dt} = -\dfrac{R_s}{L_d} i_d + \dfrac{L_q}{L_d}\omega_e i_q + \dfrac{1}{L_d} u_d \\ \dfrac{di_q}{dt} = -\dfrac{R_s}{L_q} i_q - \dfrac{L_d}{L_q}\omega_e i_d - \dfrac{1}{L_q}\omega_e\psi_f + \dfrac{1}{L_q} u_q \end{cases} \tag{5}$$

where, R_s is the motor resistance, L_d and L_q is the motor q-axis inductance, and q-axis inductanceand, respectively; and u_d and u_q is d-axis stator voltage and q-axis stator voltage, respectively; and i_d is the d-axis current.

The traditional approach in PMSM drive systems relies on a cascade control strategy using linear controllers with different bandwidths for the speed and current loops. However, this method faces challenges due to unmodeled dynamics, parameter uncertainties, and nonlinearity within the system. To address these limitations and improve dynamic performance, a non-cascade control method has emerged, enabling synchronous control of speed and current.

C. SECOND-ORDER MODEL OF A PERMANENT MAGNET SYNCHRONOUS MOTOR

Redesigning equation (4) (5) yields:

$$\begin{cases} \dot{\omega}_e = \alpha i_q - aT_L - a_1\omega_e \\ \dot{i}_q = \beta u_q - b\omega_e\psi_f - b_1 i_q + b_2\omega_e i_d \end{cases} \tag{6}$$

where, $\alpha = 3n_p\psi_f/2J$, $a = 1/J$, $a_1 = B/J$, $\beta = 1/L_q$, $b = 1/L_q$, $b_1 = R_s/L_q$, $b_2 = -L_q/L_d$. When the perturbation of motor parameter variation is considered, the above equation can be written as:

$$\begin{cases} \dot{\omega}_e = (\alpha + \Delta\alpha)i_q - (a + \Delta a)T_L - (a_1 + \Delta a_1)\omega_e \\ \dot{i}_q = (\beta + \Delta\beta)u_q - (b + \Delta b)\omega_e\psi_f - (b_1 + \Delta b_1)i_q \\ \quad + (b_2 + \Delta b_2)\omega_e i_d \end{cases} \tag{7}$$

where $\Delta\alpha$, Δa, Δa_1, $\Delta\beta$, Δb, Δb_1 and Δb_2 are perturbation terms caused by theparameter variations. Subsequently, demonstrating equation (7) as a second-order system, it can be simplified using the ultra-local model [26] as follows:

$$\begin{cases} \dot{\omega}_e = \alpha i_q^* + f_1 \\ \dot{i}_q = \beta u_q^* + f_2 \end{cases} \tag{8}$$

$$\begin{cases} f_1 = \alpha(i_q - \Delta i_q^*) - (a + \Delta a)T_L - (a_1 + \Delta a_1)\omega_e + \Delta\alpha i_q \\ f_2 = \beta(u_q - \Delta u_q^*) - (b + \Delta b)\omega_e\psi_f - (b_1 + \Delta b_1)i_q \\ \quad + (b_2 + \Delta b_2)\omega_e i_d + \Delta\beta u_q \end{cases} \tag{9}$$

where, f_1 and f_2 represent the unmodelled dynamics, unknown perturbations, and uncertainties associated with the mechanical part and q-axis of the PMSM drive system, respectively.

According to equations (8) (9):

$$\ddot{\omega}_e = \alpha(\beta u_q^* + f_2) + \dot{f}_1 \tag{10}$$

III. DESIGN OF THE CONTROLLER

A. SYSTEM DESIGN

The state variable that defines the velocity error is as follows:

$$x_1 = e = \omega_e^* - \omega_e \tag{11}$$

where, ω_e^* represents the reference rotational speed value. Define the derivative of the rotational speed as x_2 satisfying:

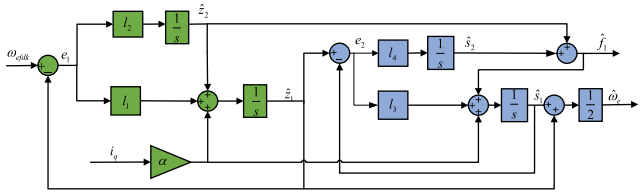

FIGURE 2. Cascaded extended state observer for observing f_1.

$x_2 = \dot{x}_1$, According to equation (10), the second-order model of the PMSM can be expressed as:

$$\begin{cases} \dot{x}_1 = x_2 + f_1 \\ \dot{x}_2 = -\alpha\beta u_q + f_2 \\ y = x_1 \end{cases} \tag{12}$$

By defining $\vec{x}_1 = x_1$ and $\vec{x}_2 = x_2 + f_1$, equation (12) can be written as:

$$\begin{cases} \dot{\vec{x}}_1 = x_2 \\ \dot{\vec{x}}_2 = -\alpha\beta u_q + \dot{f}_1 + f_2 \\ y = \vec{x}_1 \end{cases} \tag{13}$$

B. DESIGN AND STABILITY ANALYSIS OF CESO

In order to enhance the immunity performance of the servo system in the permanent magnet synchronous motor, the cascaded extended state observer (CESO) is introduced to estimate the aggregate perturbations f_1 and f_2 as mentioned in equation (13). To ensure accurate observation of f_1, a two-stage cascaded linear CESO is specifically designed in the following form:

$$\begin{cases} e_1 = z_1 - \hat{z}_1 \\ \dot{z}_1 = \alpha i_q + z_2 + l_1 e_1 \\ \dot{z}_2 = l_2 e_1 \\ e_2 = s_1 - \hat{s}_1 \\ \dot{s}_1 = \alpha i_q + s_2 + l_3 e_2 + z_2 \\ \dot{s}_2 = l_4 e_2 \\ f_1 = z_2 + s_2 \end{cases} \tag{14}$$

where z_1 and s_1 represent the estimated rotational speeds of ESO1 and ESO2, respectively. Likewise, z_2 and s_2 denote the estimated disturbances of ESO1 and ESO2, respectively. Furthermore, l_1, l_2, l_3, and l_4 are the observer gains. The specific block diagram of the cascade extended state observer for observing f_1 is depicted in figure 2.

To achieve accurate observation of f_2, the second-order linear ESO is designed in the following form:

$$\begin{cases} e_1 = x_1 - \hat{x}_1 \\ \dot{x}_1 = \beta u_q + x_2 + m_1 e_1 \\ \dot{x}_2 = m_2 e_1 \\ e_2 = \eta_1 - \hat{\eta}_1 \\ \dot{\eta}_1 = \beta u_q + \eta_2 + m_3 e_2 + x_2 \\ \dot{\eta}_2 = m_4 e_2 \\ f_2 = x_2 + \eta_2 \end{cases} \tag{15}$$

where x_1 and η_1 represent the estimated currents of ESO1 and ESO2, respectively. Similarly, x_2 and η_2 denote the estimated disturbances of ESO1 and ESO2, respectively. Additionally, m_1, m_2, m_3, and m_4 are the observer gains. The specific block diagram of the cascade extended state observer for observing f_2 is depicted in figure 3.

Theorem 1: the perturbations of the system and their derivatives estimated by the cascaded extended state observers (14) and (15) are ultimately uniformly bounded.

Proof: we will now demonstrate the stability of the chosen cascaded extended state observer (15) through the following proof.

Let $e_{ij} = e_i$, where i or $j = 1, 2$. The error equation for the second-order ESO1, which is used to observe f_2, can be derived as follows.

$$\begin{cases} \dot{e}_{11} = e_{12} - m_1 e_{11} \\ \dot{e}_{12} = h - m_2 e_{11} \end{cases} \tag{16}$$

where e_{12} be the estimation error associated with the perturbation x_2. It can be expressed as follows:

$$\dot{e}_{12} = m_2 - \hat{m}_2 \tag{17}$$

let $\gamma_i = e_{1i}/\omega_0^{i-1}$, $i = 1, 2$, which follows from equation (16):

$$\dot{\gamma} = \omega_0 H\gamma + hK/\omega_0 \tag{18}$$

where, $\gamma = \begin{bmatrix} \gamma_1 \\ \gamma_2 \end{bmatrix}$, $H = \begin{bmatrix} -2 & 1 \\ -1 & 0 \end{bmatrix}$, $K = \begin{bmatrix} 0 \\ 1 \end{bmatrix}$

Since both eigenvalues of H are -1, we can conclude that H is Hurwitz stable. As a result, there exists a unique positive definite matrix P such that:

$$H^T P + PH = -I \tag{19}$$

where, $P = \begin{bmatrix} \frac{1}{2} & -\frac{1}{2} \\ -\frac{1}{2} & \frac{3}{2} \end{bmatrix}$

The Lyapunov function is chosen as: $V(\gamma) = \gamma^T P\gamma$, then,

$$\dot{V}(\gamma) = \dot{\gamma}^T P\gamma + \gamma^T P\dot{\gamma} = -\omega_0 ||\gamma||^2 + 2\omega_0^{-1}\gamma^T PKh \tag{20}$$

Since h is globally Lipschitz with respect to x, that is, there exists a constant ζ such that $h \le \zeta \|\|x - z_{1i}\|\|$ for all x, z_{1i}, we can deduce the following relationship:

$$2\omega_0^{-1}\gamma^T PKh \le 2\zeta\omega_0^{-1}\gamma^T PK||x - z_{1i}|| \tag{21}$$

when $\omega_0 \ge 1$, we can observe that $\omega_0^{-1}||x - z_{1i}|| = \omega_0^{-1}||e_{1i}|| \le ||\gamma||$. Therefore, we have the inequality:

$$2\omega_0^{-1}\gamma^T PKh \le \rho||\gamma||^2 \tag{22}$$

where, $\rho = ||PK\zeta||^2 + 1$, by substituting equation (22) into equation (21), we obtain:

$$\dot{V}(\gamma) \le -(\omega_0 - \rho)||\rho||^2 \tag{23}$$

When $\omega_0 > \rho$, it follows that $\dot{V}(\gamma) < 0$. The same applies to e_{2i}. Thus, we can conclude that

$$\lim_{t\to\infty} e_{ij} = 0 \tag{24}$$

where, $i, j = 1, 2$

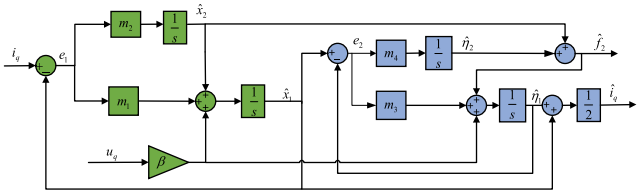

FIGURE 3. Cascaded extended state observer for observing f_2.

Based on the aforementioned analysis, it can be concluded that Lyapunov's asymptotic stability theorem holds, indicating the convergence of the cascaded extended state observer (CESO). Additionally, as the system reaches a steady state, the right-hand term of equation (16) converges to 0. Therefore, it can be inferred that:

$$\begin{cases} e_{11} = \dfrac{h}{m_2} \\ e_{12} = m_1 \dfrac{h}{m_2} \end{cases} \tag{25}$$

The observations in equation (24) demonstrate that the steady-state error is sufficiently small when the value of m_2 is significantly greater than h.

In this paper, the pole placement technique is used for the gain design of a second-order LESO, based on the pole placement technique, to achieve desired closed-loop system performance:

$$\begin{cases} m_1 = 2\omega_{c21} \\ m_2 = 2\omega_{c21}^2 \\ m_3 = 2\omega_{c22} \\ m_4 = 2\omega_{c22}^2 \end{cases} \tag{26}$$

In the given equation, ω_{c21} and ω_{c22} represent the bandwidths of the second-order LESO for estimating x_2 and η_2 respectively. It is worth noting that, with reference to the rule of thumb in [27], the CESO studied in this paper, in order to estimate signals contaminated by high-frequency noise, ESO1 chooses lower observer bandwidths to prevent noise from being over-amplified. Meanwhile, in order to estimate the signal less affected by noise, ESO2 chooses a higher observer bandwidth to maintain a higher tracking capability. Meanwhile, after several tests in the experiment, They are subject to the condition $2\omega_{c21} = \omega_{c22}$. The use of cascaded ESO in this context offers several advantages. It not only enables the estimation of x_2, η_2, and the aggregate disturbance f_2 based on measured signals, but also enhances the observation of disturbances and suppresses the amplification of noise measurements compared to conventional ESO.

In summary, the above sections cover the observer design and stability analysis for the aggregate perturbation f_2. The same procedure can be applied to the aggregate perturbation f_1, and the corresponding observer gain is as follows:

$$\begin{cases} l_1 = 2\omega_{c11} \\ l_2 = 2\omega_{c11}^2 \\ l_3 = 2\omega_{c12} \\ l_4 = 2\omega_{c12}^2 \end{cases} \tag{27}$$

where ω_{c11} and ω_{c12} represent the bandwidths of the second-order LESO for estimating z_2 and s_2 respectively. These bandwidths satisfy the condition $2\omega_{c11} = \omega_{c12}$.

C. DESIGN OF A COMPOSITE SINGLE-LOOP ANFTSMC CONTROLLER BASED ON ULTRA-LOCAL MODEL AND ITS STABILITY ANALYSIS

Considering the effects of parameter uptake and unknown perturbations, in order to achieve high-performance control of SPMSM, accelerate the speed transient response, and improve the steady state control accuracy, an ANFTSMC speed controller is designed in this section by changing the coefficients affecting the jitter term of the NFTSMC adaptively with the speed error. It can effectively reduce jitter and achieve fast convergence.

In accordance with equation (10), the composite single-loop controller can be designed as follows:

$$u_q^* = \frac{-\dot{f}_1 - \alpha f_2 + \ddot{\omega}_e + u_c}{\alpha\beta} \tag{28}$$

where u_c represents the controller output.

Let $sig^b(e) = \text{sign}(x)\,|x|^b$, the selection of a new sliding mode surface can be described as follows:

$$\sigma = e + a_1 \,\text{sig}^{b_1}(e) + a_2 \,\text{sig}^{b_2}(\dot{e}) \tag{29}$$

where $a_1 > 0$, $a_2 > 0$, $1 < b_1 < 2$, and $b_1 > b_2$.

The derivation of equation (29) is as follows:

$$\dot{\sigma} = \dot{e} + a_1 b_1 \,|e|^{b_1 - 1}\,\dot{e} + a_2 b_2 \,|\dot{e}|^{b_2 - 1}\,\ddot{e} \tag{30}$$

After selecting the NFTSM surface described by equation (29), to ensure that the state variables remain on the slip mode surface $\sigma = 0$, the equivalent control law u_e is derived from the condition $\dot{\sigma} = 0$ as:

$$u_e = \frac{1}{a_2 b_2}\,|e|^{1-b_2}\,(\dot{e} + a_1 b_1 \,|e|^{b_1 - 1}\,\dot{e}) \tag{31}$$

To facilitate the rapid convergence of the state variables to the NFTSM surface, the switching control law u_{sw} is designed as follows:

$$u_{sw} = -k_1\sigma - k_2 \,\text{sig}^g(\sigma) \tag{32}$$

where k_1 and k_2 are positive gain constants, to be further discussed later. The jitter effect is suppressed by selecting the value of g such that $0 < g < 1$, allowing the system state to smoothly approximate the dynamic sliding surface. It is important to note that a larger value of g leads to smoother switching forces, but at the expense of reduced system robustness.

To address the influence of k_2 on the jitter of u_q, we introduce an adaptive parameter k_2' for k_2 with the value:

$$k_2' = k_2 + (k_{2max} - k_2)tanh(k_s \left|\omega_e^* - \omega_e\right|) \tag{33}$$

where k_{2max} is the maximum gain, k_s is the gain, and k_2 is the minimum gain.

To design the new model-free sliding mode control law for the speed ring, we utilize the state equation (13), the equivalent control law equation (31), and the switching control law equation (32). This results in the following expression:

$$u_c = u_e + u_{sw} \tag{34}$$

In order to assess the stability of the proposed control law, we now proceed with the stability analysis. The proof of asymptotic stability for the ANFTSMC controller is analyzed as follows:

Proof: consider the following Lyapunov function for the analysis:

$$V(t) = \frac{1}{2}\sigma^2 \tag{35}$$

The first-order derivative of the Lyapunov function V(t) can be obtained from equations (29) to (32) as follows:

$$\begin{aligned} \dot{V}(t) &= \sigma\dot{\sigma} \\ &= \sigma(-k_1\sigma - k_2\,\mathrm{sgn}^g(\sigma)) \\ &= -k_1\sigma^2 - k_2|\sigma|^g\,\mathrm{sign}(\sigma) \\ &= -k_1\sigma^2 - k_2|\sigma|^{g+1} \\ &\le 0 \end{aligned} \tag{36}$$

For the aforementioned equation, it holds true that $\sigma\dot{\sigma} = 0$ if and only if $\sigma(t) = 0$.

In conclusion, the equation (36) is constant and non-positive. Hence, the designed convergence law satisfies the sliding mode reachability condition, indicating the asymptotic stability of the sliding mode controller.

The proof of local finite-time stability is as follows.

Theorem 2: If the Lyapunov function satisfies the given inequality:

$$\dot{V}(x) + \delta V(x) + \xi V^{\lambda}(x) \le 0 \tag{37}$$

where $\delta > 0$, $\xi > 0$, and $0 < \lambda < 1$.

When the system globally converges, the convergence time to 0 is given by

$$t \le \frac{1}{\delta(1-\lambda)} ln[\frac{\delta V^{1-\lambda}(x_0)}{\xi} + 1] \tag{38}$$

Convergence in finite time is proven using theorem 2 and the equations (35) and (36):

$$\begin{aligned} \dot{V} &\le -a\,|\sigma|^2 - b\,|\sigma|^{g+1} \\ &= -2aV - 2^{(g+1)/2} bV^{(g+1)/2} \\ &\le 0 \end{aligned} \tag{39}$$

So it can be written as:

$$\dot{V} + 2aV - 2^{(g+1)/2} bV^{(g+1)/2} \le 0 \tag{40}$$

Based on theorem 2 and the initial value $V(0) = V_0$, the convergence time can be bounded by the following inequality:

$$T_s \le \frac{1}{a(1-g)} ln(1 + (2V_0)^{(1-g)/2}\frac{a}{b}) \tag{41}$$

In summary, the permanent magnet synchronous motor can achieve asymptotic convergence to a desired reference position within a finite time using the control rate u_q^*. The drive framework for the permanent magnet synchronous motor based on the proposed strategy is illustrated in figure 4.

IV. EXPERIMENTAL VERIFICATION

In the experimental test, a PMSM (Permanent Magnet Synchronous Motor) control platform with a floating-point digital signal processor STM32FG474 as the control core was adopted, and we utilized a pulse-width modulation (PWM) technique with a carrier frequency of 10 kHz. The experimental platform, as shown in figure 5, consists of a 200W permanent magnet synchronous motor, a hysteresis dynamometer, a control board, a driver board, a host PC, a power supply, a current clamp, and a motor performance analyzer. Table 1 provides the motor parameters used in the experimental tests. In this case, the specific model information of the measurement equipment is shown in Table 2.

A. EFFECT OF PARAMETERS ON EXPERIMENTS

In this section, the experimental setup will undergo an abrupt change in speed from 500 RPM to 1500 RPM under no-load conditions. The main objective is to observe the impact of parameter changes on the results. The gain of the nonlinear disturbance observer, $\lambda = 6 \times 10^6$, and the parameters of the phase-locked loop are adjusted as follows: $k_{sp} = 80000$ and $k_{si} = 1 \times 10^8$. The current loop parameters are adjusted as: $k_{cp} = 0.24492$, $k_{ci} = 221$. To analyze the effect of the algorithm on the experiment, the control variable method is implemented, where only one parameter is altered at a time. The observer parameters used are as follows: $\omega_{c11} = 5$, $\omega_{c12} = 10$, $\omega_{c21} = 500$, $\omega_{c22} = 1000$, $\alpha = 7000$, $\beta = 8000$. By systematically varying one parameter while keeping others constant, we can study the isolated impact of each parameter on the overall system behavior during the experiments.

1) Effect of k_1: figure 6(a) - (d) displays the comparison curves of rotational speed, d-axis current, q-axis current, and q-axis voltage, respectively. In figure 6, the green dashed line represents the experimental result for $k_1 = 60$, the blue dashed line represents the experimental result for $k_1 = 130$, and the orange solid line represents the experimental result for $k_1 = 200$.

2) Effect of k_2: figure 7(a) - (d) illustrates the comparison curves of rotational speed, d-axis current, q-axis current, and

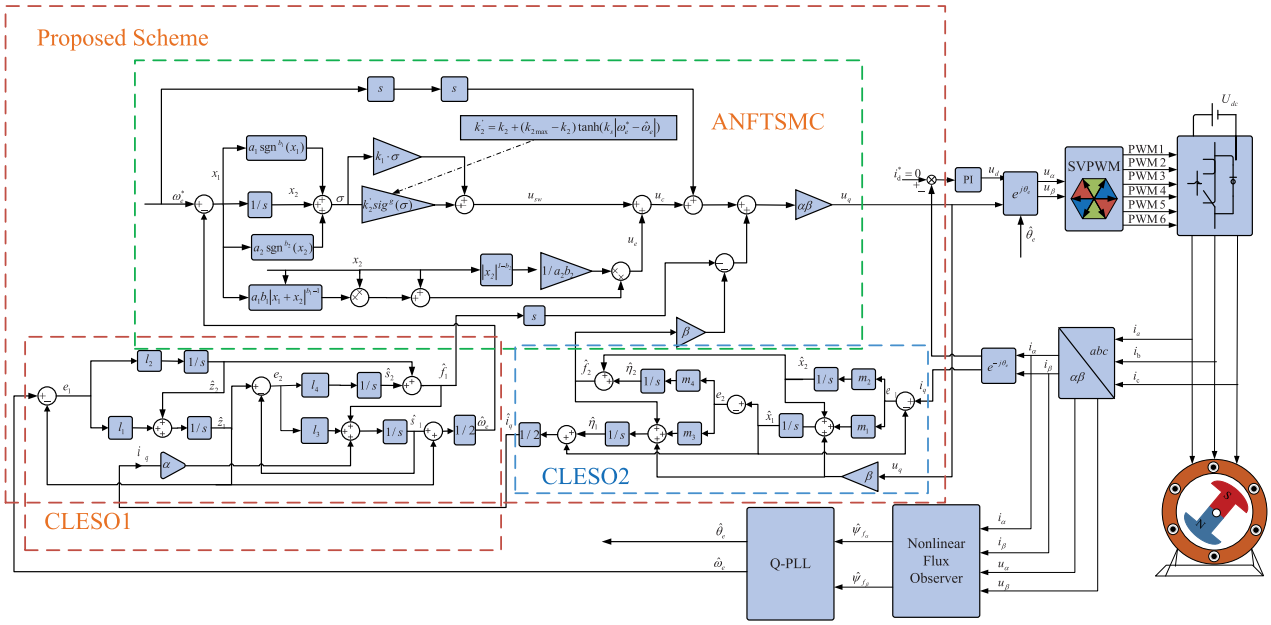

FIGURE 4. The overall control block diagram.

FIGURE 5. Block diagram of the experimental setup.

TABLE 1. Parameters of permanent magnet synchronous motor.

Parameters	Value
Pole pairs	5
q-axis inductors(mH)	0.195185
d-axis inductors(mH)	0.195185
Stator resistance(Ω)	0.35
Flux linkage (Wb)	0.0109
Rotor Moment of Inertia($kg.m^2 \times 10^-4$)	0.58
Rated Torque(N.m)	1.27
Rated Output(kw)	0.2
Rated Speed(rpm/min)	1600
Rated Voltage(V)	24
Rated Current(A)	12.5

q-axis voltage, respectively. In figure 7, the green dashed line represents the experimental result for $k_2 = 0.1$, the blue dashed line represents the experimental result for $k_2 = 0.01$, and the orange solid line represents the experimental result for $k_2 = 0.001$.

3) Effect of ω_{c11}: figure 8(a) - (d) depicts the comparison curves of rotational speed, d-axis current, q-axis current, and q-axis voltage, respectively. In figure 8, the green dashed line represents the experimental result for $\omega_{c11} = 2$, the blue dashed line represents the experimental result for $\omega_{c11} = 5$, and the orange solid line represents the experimental result for $\omega_{c11} = 15$.

4) Effect of ω_{c21}: figure 9(a) - (d) illustrates the comparison curves of rotational speed, d-axis current, q-axis current, and q-axis voltage, respectively. In figure 9, the green dashed line represents the experimental result for $\omega_{c21} = 200$, the blue dashed line represents the experimental result for $\omega_{c21} = 500$, and the orange solid line represents the experimental result for $\omega_{c21} = 800$.

Based on the above results, we can draw the following conclusions regarding the impact of different parameter values on the system's performance. Smaller values of k_1 lead to faster voltage and speed tracking speed but may cause overshooting and an increase in transient q-axis current at the initial moment. On the other hand, larger values of k_2 result in faster tracking speed and help suppress the transient q-axis current at the initial moment. Increasing the value of ω_{c11} leads to a faster response; however, it also results in a relatively large transient q-axis current when the speed undergoes sudden changes. Additionally, smaller values of ω_{c21} allow the system to reach steady-state faster, but they may also lead to overshooting. In summary, these parameter values significantly impact the system's performance, influencing aspects such as speed tracking, transient current behavior, and response speed.

B. COMPARISON EXPERIMENT

The effectiveness of the method is validated through comparative experiments involving the Cascaded Extended State Observer-based Adaptive Non-singular Fast Sliding Mode Controller (CO-ANFTSMC), PID, and SMC. The output of

TABLE 2. Equipment model/specification.

Equipment	Model/Specification
MOSFET	Infineon NTMFS5C430NL (40 V, 1.4 mΩ, 200 A)
MOSFET Driver IC	TI DRV8302
Controller	STM32FG474
Oscilloscope	RIGOL DS1104Z Plus (4-channel, 100MHz, 1GSa/s)
Motor Performance Analyzer	Weiheng Technology WH6501
Hysteresis Graph Tester	Weiheng Technology ZC Series
Power Supply	MAISHENG MS-605D
Current Clamp	Hantek CC65 AC/DC
Motor Model	PMSM HN7J-060430D1KUAA

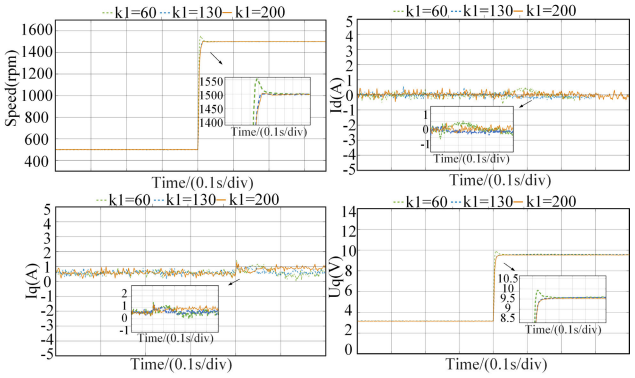

FIGURE 6. Comparison curves for different k_1 values. (a) Speed response results. (b) i_d results. (c) i_q response results. (d) u_q response results.

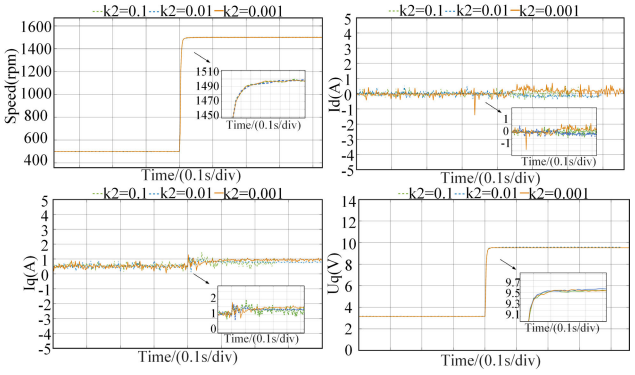

FIGURE 7. Comparison curves for different k_2 values. (a) Speed response results. (b) i_d results. (c) i_q response results. (d) u_q response results.

the SMC controller can be represented as follows:

$$\dot{i}_q^* = \frac{3n_p\psi_f}{2J}\left[c(-\dot{\omega}_e) + msign(c(\omega_e^* - \omega_e) - \dot{\omega}_e)\right] + q(c(\omega_e^* - \omega_e) - \dot{\omega}_e) \quad (42)$$

The experimental parameters for CO-ANFTSMC, PID, and SMC are designed as shown in Table 3, respectively.

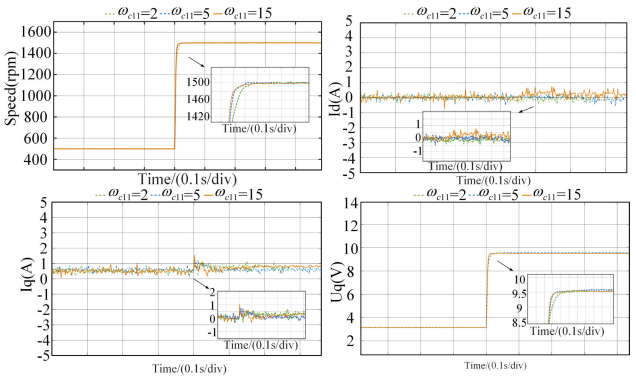

FIGURE 8. Comparison curves for different ω_{c11} values. (a) Speed response results. (b) i_d results. (c) i_q response results. (d) u_q response results.

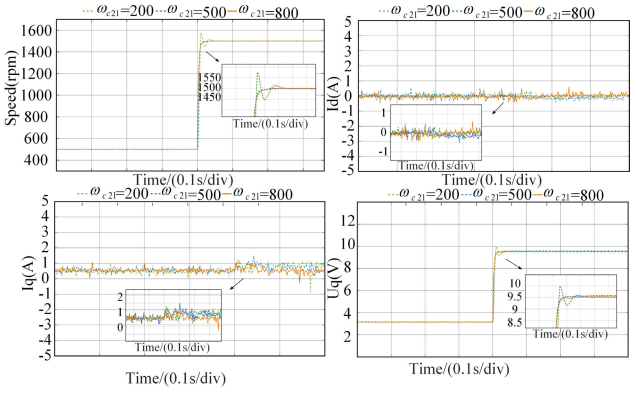

FIGURE 9. Comparison curves for different ω_{c21} values. (a) Speed response results. (b) i_d results. (c) i_q response results. (d) u_q response results.

The parameters of the PI controller can be designed as:

$$k_p = L/2T, k_i = R/2T \quad (43)$$

$$k_{cp} = 3J/(5T_{d2}k_t), k_{ci} = 3J/(25T_{d2}^2k_t) \quad (44)$$

$$k_{sp} = 2\zeta\omega_n, k_{si} = \omega_n^2 \quad (45)$$

where $T_{d2} = T_d + 2T$, T is the interrupt period, and k_t is the torque constant, ζ is the damping coefficient, and ω_n is the natural frequency.

The parameters in the SMC can be set as follows:

$$2J/(3P_n\psi_f) * qc = k_{cp}2J/(3P_n\psi_f) * (q + c) = k_{ci} \quad (46)$$

Because a lot of simulation tests have been performed in Matlab/simulink before doing the experiment. So the parameter selection of CO-ANFTSMC please follow the following rules:

The selection of the sliding mould surface parameters directly affects the stability of the motor control system. The a_1 and a_2 approximation parameters are selected to confirm the system stability and then fine-tuned. a1 becomes larger, leading to transient overshooting of the system, and the current and torque are affected. a1 becomes smaller, leading to slower speed response and longer time to reach

TABLE 3. Experimental parameters for PI, SMC, CO-ANFTSMC.

PI	SMC	CO-ANFTSMC
k_p=0.02	c=3	a_1=2.5
k_i=0.365	q=320	a_2=0.3
	m=20	b_1=1.5
		b_2=1.4
		k_1=130
		k_2=0.01
		g=0.1

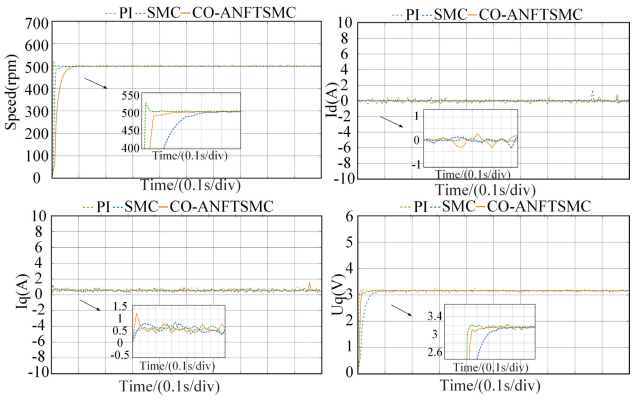

FIGURE 10. Comparison curves with different controllers during the start-up phase. (a) Speed response results. (b) i_d results. (c) i_q response results. (d) u_q response results.

the given values. In contrast to a_1, a larger a_2 will result in a slower speed response, while a smaller a_2 will result in system oscillations and will not guarantee motor control performance.

The choice of parameters for the NFTSM control law affects the slip surface arrival time. Compared with the traditional exponential convergence law, k_1 will speed up the dynamic response and reach the given speed earlier, but too high a speed will make the speed in the transient steady state process serious jitter, current and torque waveforms are distorted; and a small gain will make the speed response time longer, affecting the dynamic response speed. Adjusting the maximum and minimum values of k_2 at this point can ameliorate this problem by accelerating convergence while reducing jitter.

Although the parameters of SMC, PI, and CO-ANFTSMC can be calculated by the above method, the coefficients need to be adjusted according to the operation effect in the actual debugging.

The experiments are divided into three groups. The first group consists of comparison curves of the permanent magnet synchronous motor during the starting stage. The second group includes comparison curves under sudden increases and decreases of rotational speed. Lastly, the third group comprises comparison curves under sudden changes in load during steady-state conditions.

1) Start-up phase: The reference speed is set to 500 r/min, and the motor starts with no load. figure 10(a) - (d) show

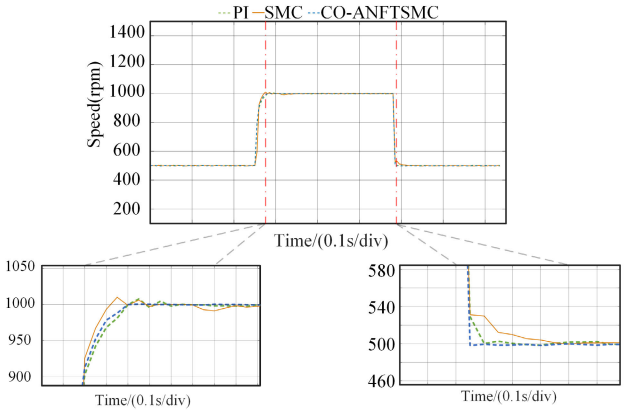

FIGURE 11. Speed comparison curves with different controllers under sudden speed change.

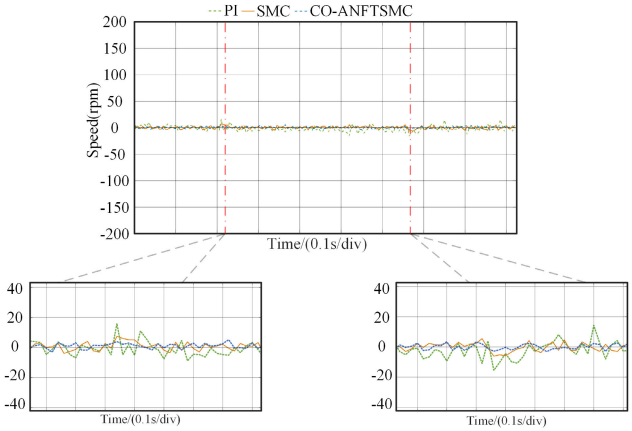

FIGURE 12. Comparison of speed error for different schemes under speed command variation.

the speed, i_d, i_q, and u_q response curves, respectively. It is evident from Fig. 10 that CO-ANFTSMC achieves faster speed tracking compared to PID and SMC. Moreover, the d-axis current, q-axis current, and q-axis voltage exhibit significantly smaller fluctuations under CO-ANFTSMC control compared to PID and SMC control. Furthermore, CO-ANFTSMC effectively mitigates the transient current at the initial moment.

2) Sudden speed increase and decrease phases: The speed response curves are displayed in figure 11, and concurrently, the speed error curve is presented in figure 12. It can be observed from figure 11 to figure 12 that CO-ANFTSMC demonstrates a faster response and relatively smaller speed fluctuations during sudden speed increases and decreases, as compared to PID and SMC.

3) Sudden load torque phase: The speed response curve is shown in figure 13 when the load undergoes a sudden change. During loading, the torque changes from 0 to 1 N.m, and during unloading, the torque changes from 1 N.m to 0. The use of CO-ANFTSMC results in a quicker return of the PM synchronous motor system to the steady state, compared to PID and SMC.

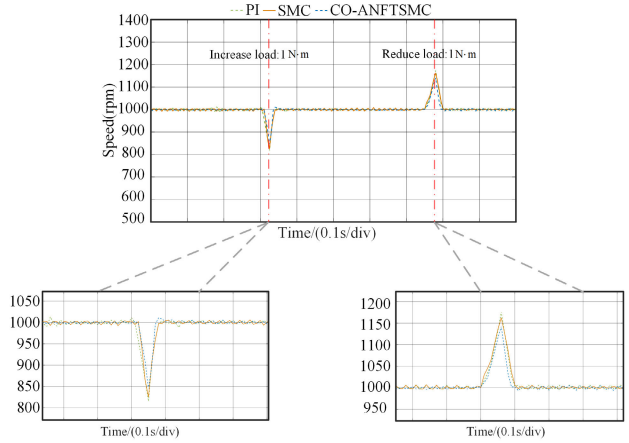

FIGURE 13. Speed comparison curves under different controllers for sudden loading and unloading.

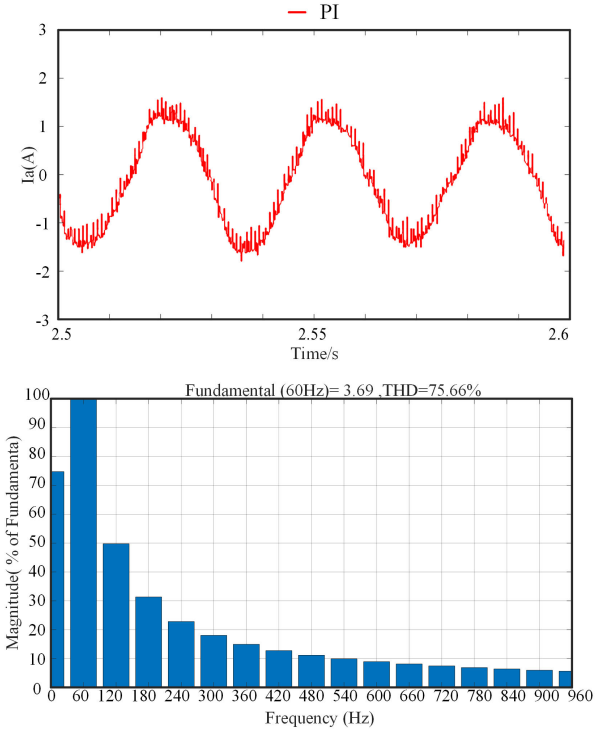

FIGURE 14. THD analysis of PI's A phase stator current.

4) One current cycle of phase A is selected for harmonic analysis. From the THD of phase A current in figure 14-16, it can be seen that the THD of PI, NFTSMC, and IST-NFTSMC are 75.66%, 58.08%, and 52.05%, respectively. The comparative results indicate that CO-ANFTSMC is more effective in suppressing harmonics other than the fundamental, compared to PID and SMC.

In conclusion, CO-ANFTSMC shows excellent performance in terms of anti-interference performance, dynamic response and robustness compared to SMC and PID. In addition, CO-ANFTSMC effectively suppresses transient currents at the initial moment.

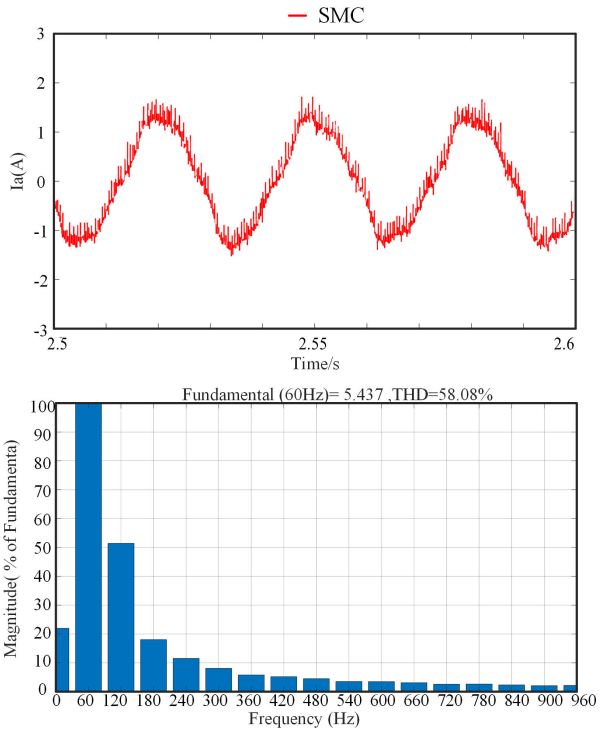

FIGURE 15. THD analysis of SMC's A phase stator current.

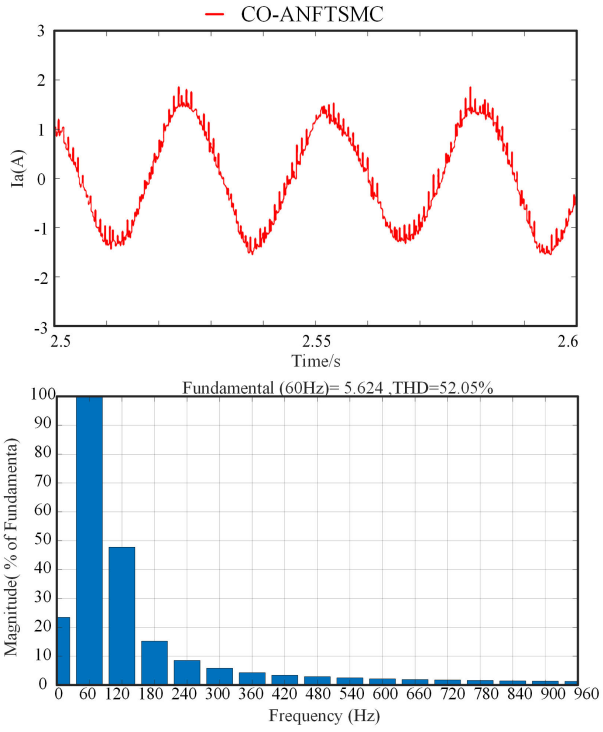

FIGURE 16. THD analysis of CO-ANFTSMC's A phase stator current.

V. CONCLUSION

Aiming at the problem of dynamic performance degradation and static deviation increase due to parameter mismatch in the

cascade control structure of permanent magnet synchronous motors, a CESO-based SPMSM speed-current single-loop control method is proposed. By comparing the experiments of PI and SMC under different working conditions and analysing the experimental results, conclusions are drawn:

(1) The CESO-based ANFTSMC speed controller is designed to restore the motor speed, current and torque to the given values in a very short time under motor parameter ingress and unknown perturbations, which improves the response speed and robustness of the system; and, compared with the PID and SMC controls, the d-axis current, q-axis current and q-axis voltage fluctuations are significantly smaller, effectively suppressing the transient current at the initial moment; CESO is designed to feedback the unknown part of external disturbances to the controller for compensation and suppress the amplification of noise measurements.

(2) Through the comprehensive comparison with PI and SMC control algorithms, it is verified that the algorithm still has high accuracy control performance under different working conditions such as motor parameters and load time-varying regimes, and weakens the system jitter and strengthens the robustness of the system while guaranteeing the system reliability and safety.

(3) The bandwidth of the controller is improved by using the non-serial structure control method. In addition, due to the large number of parameters, how to accurately design the parameters theoretically and smoothly extend them to engineering is a future work to be done.

REFERENCES

[1] K. Lin, P. Lin, and B. Yang, "Two-degree-of-freedom control with linear extended state observer for PMSM drive system," in *Proc. 41st Chin. Control Conf. (CCC)*, Hefei, China, Jul. 2022, pp. 2779–2784.

[2] Y.-C. Kwon, S.-K. Sul, N. A. Baloch, S. Morimoto, and M. Ohto, "Design, modeling, and control of an IPMSM with an asymmetric rotor and search coils for absolute position sensorless drive," *IEEE Trans. Ind. Appl.*, vol. 52, no. 5, pp. 3839–3850, Sep. 2016.

[3] X. Song, J. Fang, B. Han, and S. Zheng, "Adaptive compensation method for high-speed surface PMSM sensorless drives of EMF-based position estimation error," *IEEE Trans. Power Electron.*, vol. 31, no. 2, pp. 1438–1449, Feb. 2016.

[4] J. Zhu, Q. Ge, and P. Sun, "Extended state observer-based sensorless control for high-speed Maglev application in single-feeding mode and double-feeding mode," *IEEE Trans. Transport. Electrific.*, vol. 8, no. 1, pp. 1350–1361, Mar. 2022.

[5] S. Chen, W. Ding, X. Wu, L. Huo, R. Hu, and S. Shi, "Sensorless control of IPMSM drives using high-frequency pulse voltage injection with random pulse sequence for audible noise reduction," *IEEE Trans. Power Electron.*, vol. 38, no. 8, pp. 9395–9408, Aug. 2023.

[6] Q. Tang, A. Shen, X. Luo, and J. Xu, "PMSM sensorless control by injecting HF pulsating carrier signal into ABC frame," *IEEE Trans. Power Electron.*, vol. 32, no. 5, pp. 3767–3776, May 2017.

[7] Y. Zuo, C. Lai, and K. L. V. Iyer, "A review of sliding mode observer based sensorless control methods for PMSM drive," *IEEE Trans. Power Electron.*, vol. 38, no. 9, pp. 11352–11367, Sep. 2023.

[8] S. Ye and X. Yao, "An enhanced SMO-based permanent-magnet synchronous machine sensorless drive scheme with current measurement error compensation," *IEEE J. Emerg. Sel. Topics Power Electron.*, vol. 9, no. 4, pp. 4407–4419, Aug. 2021.

[9] X. Sun, Y. Zhang, X. Tian, J. Cao, and J. Zhu, "Speed sensorless control for IPMSMs using a modified MRAS with gray wolf optimization algorithm," *IEEE Trans. Transport. Electrific.*, vol. 8, no. 1, pp. 1326–1337, Mar. 2022.

[10] T. Tarczewski and L. M. Grzesiak, "Constrained state feedback speed control of PMSM based on model predictive approach," *IEEE Trans. Ind. Electron.*, vol. 63, no. 6, pp. 3867–3875, Jun. 2016.

[11] X. Wu, Z.-Q. Zhu, and N. M. A. Freire, "High frequency signal injection sensorless control of finite-control-set model predictive control with deadbeat solution," *IEEE Trans. Ind. Appl.*, vol. 58, no. 3, pp. 3685–3695, May 2022.

[12] S. M. N. Ali, M. J. Hossain, D. Wang, K. Lu, P. O. Rasmussen, V. Sharma, and M. Kashif, "Robust sensorless control against thermally degraded speed performance in an IM drive based electric vehicle," *IEEE Trans. Energy Convers.*, vol. 35, no. 2, pp. 896–907, Jun. 2020.

[13] J. Mao, H. Li, L. Yang, H. Zhang, L. Liu, X. Wang, and J. Tao, "Non-cascaded model-free predictive speed control of SMPMSM drive system," *IEEE Trans. Energy Convers.*, vol. 37, no. 1, pp. 153–162, Mar. 2022.

[14] X. Zhang, Z. Wang, X. Li, and J. Bian, "Non-cascaded predictive speed synchronous control of dual permanent magnet motor system without weight coefficient tuning," in *Proc. 33rd Chin. Control Decis. Conf. (CCDC)*, Kunming, China, May 2021, pp. 5701–5706.

[15] H. Li, S. Wang, Y. Xie, S. Zheng, and P. Shi, "Virtual reference-based fuzzy noncascade speed control for PMSM systems with unmatched disturbances and current constraints," *IEEE Trans. Fuzzy Syst.*, vol. 31, no. 12, pp. 4249–4261, Dec. 2023.

[16] J. Mao, H. Li, Y. Zhou, L. Yang, and J. Huang, "Direct speed composite control of SPMSM drive system," *IEEE J. Emerg. Sel. Topics Power Electron.*, vol. 11, no. 5, pp. 5120–5130, Oct. 2023.

[17] X. Liu, H. Yu, J. Yu, and L. Zhao, "Combined speed and current terminal sliding mode control with nonlinear disturbance observer for PMSM drive," *IEEE Access*, vol. 6, pp. 29594–29601, 2018.

[18] A. Apte, U. Thakar, and V. Joshi, "Disturbance observer based speed control of PMSM using fractional order PI controller," *IEEE/CAA J. Autom. Sinica*, vol. 6, no. 1, pp. 316–326, Jan. 2019.

[19] W. Deng, C. Xia, Y. Yan, Q. Geng, and T. Shi, "Online multiparameter identification of surface-mounted PMSM considering inverter disturbance voltage," *IEEE Trans. Energy Convers.*, vol. 32, no. 1, pp. 202–212, Mar. 2017.

[20] L. Tian, Y. Liu, J. Zhao, and J. Sun, "The sensorless control of IPMSM based on improved sliding-mode observer," in *Proc. 27th Chin. Control Decis. Conf. (CCDC)*, Qingdao, China, May 2015, pp. 6091–6096.

[21] T. T. Phuong, K. Ohishi, and Y. Yokokura, "Advanced wideband sensorless force control based on harmonic estimation integrated singular spectrum analysis based disturbance observer," in *Proc. IECON 45th Annu. Conf. IEEE Ind. Electron. Soc.*, Lisbon, Portugal, Oct. 2019, pp. 3591–3596.

[22] N. Yang, S. Zhang, X. Li, and X. Li, "A new model-free deadbeat predictive current control for PMSM using parameter-free Luenberger disturbance observer," *IEEE J. Emerg. Sel. Topics Power Electron.*, vol. 11, no. 1, pp. 407–417, Feb. 2023.

[23] X. Liu and H. Yu, "Continuous adaptive integral-type sliding mode control based on disturbance observer for PMSM drives," *Nonlinear Dyn.*, vol. 104, no. 2, pp. 1429–1441, Apr. 2021.

[24] T. Li, X. Liu, and H. Yu, "Backstepping nonsingular terminal sliding mode control for PMSM with finite-time disturbance observer," *IEEE Access*, vol. 9, pp. 135496–135507, 2021.

[25] P. Wang, S. Li, and H. Zhu, "PMSM control based on the new nonsingular fast terminal sliding mode control algorithm," in *Proc. 40th Chin. Control Conf. (CCC)*, Shanghai, China, Jul. 2021, pp. 577–582.

[26] M. Fliess and C. Join, "Model-free control," *Int. J. Control*, vol. 86, no. 12, pp. 2228–2252, 2013.

[27] K. Łakomy and R. Madonski, "Cascade extended state observer for active disturbance rejection control applications under measurement noise," *ISA Trans.*, vol. 109, pp. 1–10, Mar. 2021.

LIJUN CHEN (Student Member, IEEE) received the bachelor's degree in electrical engineering from the Shanxi Energy College, Shanxi, China, in 2021. He is currently pursuing the master's degree with the School of Automation, Hangzhou Dianzi University, Hangzhou.

His current research interests include sensorless control, parameter identification, and model predictive control of permanent magnet synchronous motors based on unmanned aerial vehicles.

DONGLIANG LIU received the Ph.D. degree in control theory and control engineering from Zhejiang University, in 2005.

From 2005 to 2007, he was engaged in the research of ac servo motor and control in the postdoctoral workstation of the Wolong Holding Group. He has been engaged in the research and development of nonlinear control strategy, permanent magnet ac servo drive control systems, electric drive systems for electric vehicles, electric aviation, electric ship propulsion, new energy, and its related power electronics applications. His 15 papers have been published, of which, three are SCI indexed, and ten are EI indexed. From 2019 to 2022, he was the Chairperson of the National Natural Science Foundation of China (NSFC) Project "NVH Global Optimization and Control of Electric Vehicle Electric Powertrain under Multi-Service Behavior." From 2013 to 2016, he was the Host of the National Natural Science Foundation of China (NSFC) Project "Sensorless Integration Technology of Permanent Magnet Synchronous Motor and High-Efficiency Operation." From 2013 to 2016, undertook the provincial key natural science foundation project "Research on the efficient operation of permanent magnet synchronous motor for electric vehicles and its key technology" as a moderator. His research interests include electric motors and their control, new energy and power electronics/electric vehicle drive systems, electric aviation drive systems, and electric ship propulsion systems.

MINCHEN ZHU received the Ph.D. degree in control theory and control engineering from Zhejiang University, in 2020. His research interests include electric machines and their control, new energy and power electronics/electric vehicle drive systems, electric aviation drive systems, and electric ship propulsion systems.

LILI CUI received the degree from the Inner Mongolia University of Technology, in 2003. She is currently a Lecturer with Hangzhou Dianzi University, specializing in power electronics and motor control and drive applied in the direction of unmanned aerial vehicles and electric vehicles.

LIMIN SUN received the bachelor's degree in electrical engineering and automation from the Department of Electrical Engineering, School of Information Engineering, Hangzhou Dianzi University, Zhejiang, in 2017. He is currently pursuing the master's degree with Hangzhou Dianzi University. His research interest includes control strategies for permanent magnet synchronous motors, particularly focusing on lock pitch control and parameter identification based on unmanned aerial vehicles.

CHENGGEN ZHAN received the B.S. degree in automation from the Anhui University of Technology, in 2016. He is currently pursuing the master's degree in control science and engineering with Hangzhou Dianzi University. His research interests include control strategies on permanent magnet synchronous motors. Especially for flux-weakening control on permanent magnet synchronous motors on electric vehicles.

HENG SHI received the bachelor's degree in automation from the Department of Automation, Lanzhou Jiaotong University, Gansu, China, in 2016. She is currently pursuing the master's degree with Hangzhou Dianzi University. Her research interest includes the control strategies of permanent magnet synchronous motors, especially motor control and drives based on UAVs.